nature communications

Article

https://doi.org/10.1038/s41467-023-39753-2

Tunably strained metallacycles enable modular differentiation of aza-arene C–H bonds

Received: 15 May 2023

Accepted: 23 June 2023

Published online: 06 July 2023

Check for updates

Longlong Xi[1,2], Minyan Wang[1,2], Yong Liang[1], Yue Zhao[1] & Zhuangzhi Shi[1]

The precise activation of C–H bonds will eventually provide chemists with transformative methods to access complex molecular architectures. Current approaches to selective C–H activation relying on directing groups are effective for the generation of five-membered, six-membered and even larger ring metallacycles but show narrow applicability to generate three- and four-membered rings bearing high ring strain. Furthermore, the identification of distinct small intermediates remains unsolved. Here, we developed a strategy to control the size of strained metallacycles in the rhodium-catalysed C–H activation of aza-arenes and applied this discovery to tunably incorporate the alkynes into their azine and benzene skeletons. By merging the rhodium catalyst with a bipyridine-type ligand, a three-membered metallacycle was obtained in the catalytic cycle, while utilizing an NHC ligand favours the generation of the four-membered metallacycle. The generality of this method was demonstrated with a range of aza-arenes, such as quinoline, benzo[*f*]quinolone, phenanthridine, 4,7-phenanthroline, 1,7-phenanthroline and acridine. Mechanistic studies revealed the origin of the ligand-controlled regiodivergence in the strained metallacycles.

Due to the near universal advantage of C − H bonds in organic molecules, the C − H activation strategy provides an opportunity to functionalize any carbon centre in an atom-economical and streamlined way[1–10]. Because organic molecules typically contain multiple C − H bonds with comparable strengths and steric environments, regiocontrol has been a long-standing challenge within this type of chemistry[11]. The differentiation of C − H bonds is traditionally dominated by steric and electronic effects[12], and there have been considerable efforts to utilize directing groups in less constrained molecules (Fig. 1a)[13–17]. Directed C − H activation is thermodynamically favoured through conformationally rigid five-, six-, and seven-membered metallacyclic intermediates. Several elegant methods have been exploited to achieve the *meta*- and *para*-selective C − H activation of arenes through chelation-assisted macrocyclic complexes by directing groups[18–22]. Despite these advances, the generation of highly strained metallacycles in directed C − H activation remains much desired but more challenging.

Substantial progress has been made regarding the C–H activation of aliphatic amines through strained metallacycles, allowing for site-selective functionalization at the α or β position of the amino group in one catalytic step[23,24]. Early transition metals, including titanium, tantalum and zirconium, enable the hydroaminomethylation of alkenes with unprotected N-heterocycles and amines through metallaaziridine intermediates, affording either linear or branched products (Fig. 1b)[25–30]. A series of C–H functionalizations of aliphatic amines have been developed by palladium catalysis, showing β-selectivity through a four-membered ring cyclopalladation pathway (Fig. 1c)[31–33]. Compared to small aliphatic metallacycles, the formation of benzo-fused analogues comes with larger ring strain. We questioned whether such metallacycles could be

[1]State Key Laboratory of Coordination Chemistry, Chemistry and Biomedicine Innovation Center (ChemBIC), School of Chemistry and Chemical Engineering, Nanjing University, Nanjing, China. [2]These authors contributed equally: Longlong Xi, Minyan Wang. e-mail: shiz@nju.edu.cn

https://doi.org/10.1038/s41467-023-39753-2

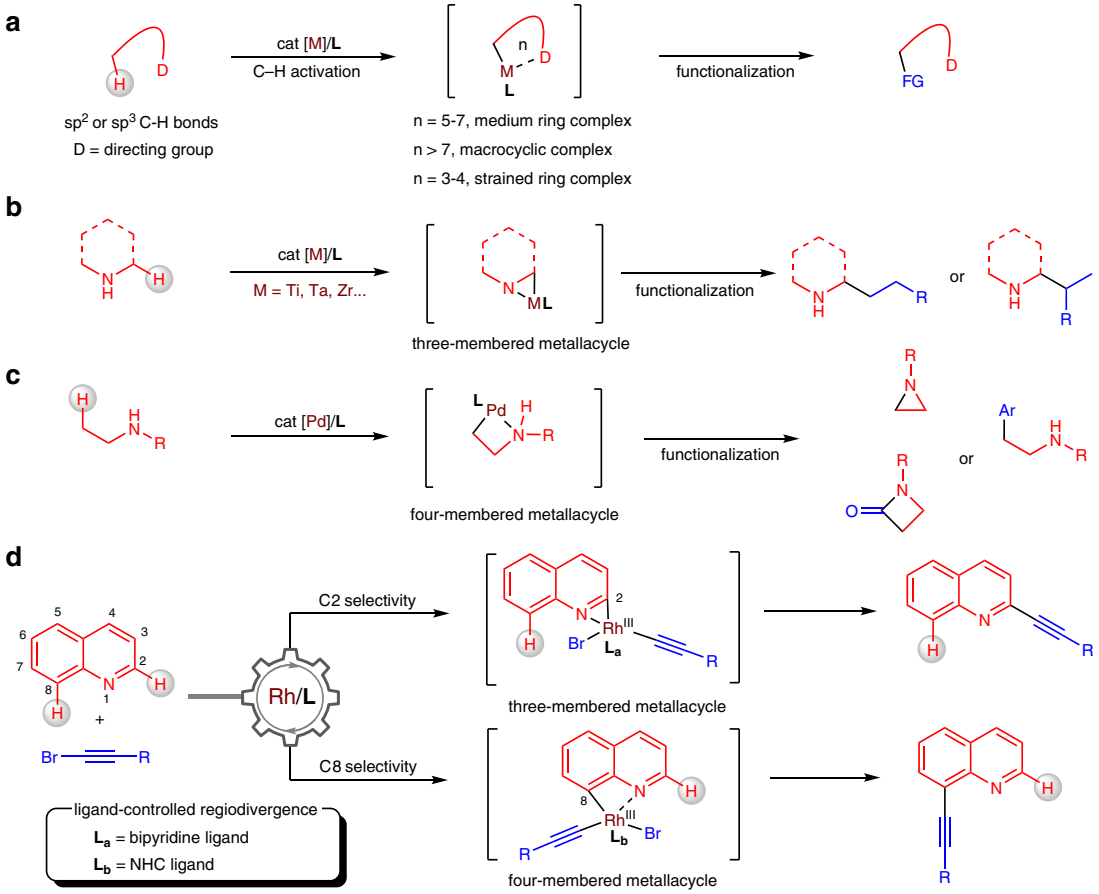

Fig. 1 | Background and discovery. a General procedures for selective C–H activation assisted by directing groups. **b** α-Selective C–H functionalization of aliphatic amines via metallaaziridine intermediates. **c** β-Selective C–H functionalization of aliphatic amines via four-membered metallacycles. **d** Modular differentiation of quinolines by tunable three- and four-membered ring cyclometallation.

generated through chelation with inherent nitrogen atoms in aza-arenes. Furthermore, switching the ring size in a unifying system to differentiate of two C–H bonds would likely have a broad impact on the continued advancement of this field.

As a representative example of bicyclic aza-arenes, quinoline contains seven C – H bonds in the pyridine (C2 to C4) and benzene (C5 to C8) cores that can be functionalized[34,35]. Structural modification of the pyridine ring has been achieved by taking advantage of strong electronic and steric bias[36–43]. An indirect route to access the benzene core involves the oxidation of quinoline to its *N*-oxide, followed by oxygen-directed C – H functionalization and subsequent reduction to the desired products[44–46]. To provide more flexibility to access the benzene core, metal clusters and dimers such as $Os_3(CO)_{10}$[47], $Ru_3(CO)_{12}$[48], and $Rh_2(OAc)_4$[49] have been employed in C – H activation through bridged metal-metal bonds. Enabled by bimetallic palladium catalysis, Yu and coworkers also designed a class of remote-directing template for differentiation of C – H bonds (C5-C7) at the benzene core of quinolines[50–53].

Here, we report the successful realization of a strategy for regiodivergent C–H activation of aza-arenes enabled by tunably strained metallacycles under monomeric rhodium catalysts (Fig. 1d). The precise differentiation of two C–H bonds proceeds through a switchable three- or four-membered-ring cyclometallation pathway by just tuning the structure of the ligands. Incorporation of alkyne motifs into aza-arenes are valuable transformations to build C–C bonds and provide a versatile handle for further modifications.

Results

Reaction design

As shown in Fig. 2, we first evaluated the reaction of 3-methylquinoline (**1a**) with (bromoethynyl)triisopropylsilane (**2a**). After treatment of $[Rh(cod)Cl]_2$ (5 mol%) with NaO^{t}Bu (2.5 equiv) at 120 °C under an Ar atmosphere in toluene, the desired product **3aa** was generated in trace amounts after 12 h (entry 1). After screening a variety of ligands for optimization (for the details of the reaction optimization, see the Supplementary Information), the optimized conditions for C2-alkynylation were determined, using 10 mol% dtbpy as a ligand. Under these conditions, product **3aa** was afforded in 84% yield, showing 99/1 *r.r.* of the C2 to C8 positions (entry 2). Interestingly, employing NHC ligands[54] resulted in a preference for C8 selectivity, and the use of IMes·HCl led to the formation of product **4aa** in 70% yield (C8/C2 = 91/9 *r.r.*) (entry 3). Employment of $[Rh(cod)Cl]_2$ with the optimal ligands resulted in the production of two rhodium complexes, Rh(cod)(dtbpy)Cl and Rh(cod)(IMes)Cl, both of which were unambiguously assigned by X-ray crystallography. Utilizing the pregenerated Rh(cod)(dtbpy)Cl as the catalyst showed a much lower reactivity than the in situ generation of the catalyst (entry 4). In contrast, the use of Rh(cod)(IMes)Cl as the catalyst improved the generation of **4aa** to 85% yield with 92/8 *r.r.* (entry 5).

Scope of the methodology

The scope of the regiodivergent C–H alkynylation was then examined (Fig. 3). In general, a series of commercially available quinolines

https://doi.org/10.1038/s41467-023-39753-2

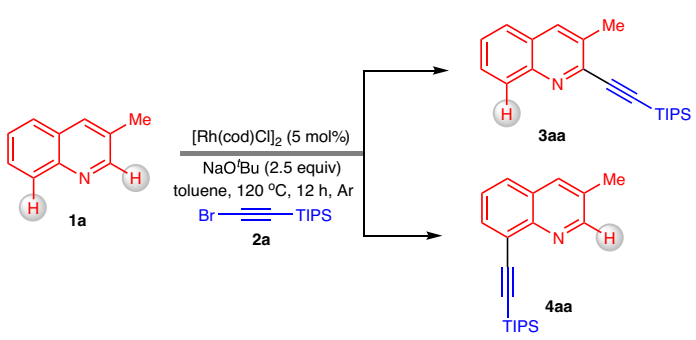

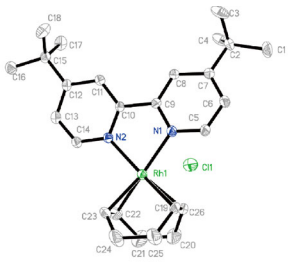

X-ray structure of Rh(cod)(dtbpy)Cl

Entry	Deviation	Yield of **3aa** (C2/C8)	Yield of **4aa** (C8/C2)
1	none	< 5% (99/1 *r.r.*)	-
2	addition of dtbpy (10 mol%)	84% (99/1 *r.r.*)	-
3	addition of IMes•HCl (10 mol%)	-	70% (91/9 *r.r.*)
4	using Rh(cod)(dtbpy)Cl (10 mol%) as catalyst	52% (99/1 *r.r.*)	-
5	using Rh(cod)(IMes)Cl (10 mol%) as catalyst	-	85% (92/8 *r.r.*)

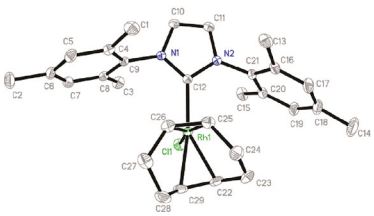

X-ray structure of Rh(cod)(IMes)Cl

Fig. 2 | Effect of the ligands on reactivity and regioselectivity. The regioselectivity ratio (r.r.) was determined by GC–MS analysis of the reaction mixtures. dtbpy = 4,4′-di-tert-butyl-2,2′-bipyridine. IMes =1,3-bis (2,4,6-trimethylphenyl)−1,3-dihydro-2H-imidazol-2-ylidene.

with varied substituents reacted smoothly with bromoalkyne **2a**, yielding two types of alkynylation products under reaction conditions A and B. The reaction of quinoline (**1b**) with bromoalkyne **2a** underwent C2- and C8-selective C−H alkynylation, providing products **3ba** (98/2 *r.r.*) and **4ba** (89/11 *r.r.*) with excellent regioselectivities. The quinolines that incorporated electron-donating groups, including phenyl (**1c**), ether (**1d-e**), silyloxy (**1 f**), and amino (**1g-h**) groups, at different positions were readily tolerated with bromoalkyne **2a** to produce the corresponding products **3ca-ha** and **4ca-ha** with excellent regioselectivity under both reaction conditions. Halide-containing quinolines **1i-p** bearing F, Cl, Br, and even I motifs were compatible with the generation of both the C2 and C8 alkynylation products. Among them, substrates **1k-l** containing substituents at the C7 position did not sterically block the reaction at the C8 position. Quinoline **1q** bearing a CF_3 group was also compatible with both sets of reaction conditions, affording **3qa** and **4qa** in 87% and 64% yields, respectively. The use of 6-cyanoquinoline (**1r**) under condition A became too sluggish to provide product **3ra**, but this substrate did not interfere with productive C−H alkynylation at the C8 position. Quinoline **1 s**, containing a phenylethynyl motif at the C3 position inhibited the reactivity at the C2 position but enabled C8-selective C−H alkynylation to generate product **4sa**. As a bidentate nitrogen ligand, 2,2′-biquinoline (**1t**) could also engage under reaction conditions B to deliver the expected products **4ta** in a good yield. We further explored the scope of alkynyl bromides with quinoline **1a**. Compared to reagent **2a**, the reaction of TIPS-protected ethynyl chloride (**2a′**) showed much lower reactivity in both reaction systems. Alkynylation with propargyl silyl ethers **2b-c** afforded the desired products in significantly lower yields, but maintained the excellent regioselectivity. Alkynyl bromides **2d** with a less sterically hindered phenyl group were problematic under both reaction conditions, and the corresponding products **3ad** and **4ad** were observed in only trace amounts. The poor outcomes are attributed to the lower stability of these bromoalkynes without TIPs group under the reaction conditions[55–59].

Other aza-arenes commonly featured in bioactive molecules and functional materials were next targeted. Benzo[*f*]quinoline (**5a**) was first employed in the catalytic systems and gave desired products **6aa** and **7aa** at the C3 and C5 positions, respectively (Fig. 4a). Phenanthridine (**5b**), the key aromatic unit of many DNA stains, underwent regiodivergent C−H alkynylation at the C6 and C4 positions in high yields with excellent selectivities (Fig. 4b). Treatment of 4,7-phenanthroline (**5c**) containing two azine motifs under reaction conditions A afforded a promising mixture of mono- and di-substituted products **6ca** and

6ca′ with a high regioselectivity (Fig. 4c). Similarly, the two products **7ca** and **7ca′** were also generated under reaction conditions B with excellent regioselectivity. Notably, the products with one or two alkynyl motifs could be separated by column chromatography on silica. When 1,7-phenanthroline (**5d**) was treated under reaction conditions A, C−H alkynylation occurred at the C8 position. However, an unusual C10-functionalized product **7da′** was obtained under reaction conditions B, indicating that C−H metalation process preferred to undergo five-membered metallacyclic intermediate (Fig. 4d). Finally, acridine (**5e**), bearing two C−H bonds (C4 and C5) for activation, gave only the monosubstituted product **7ea** in 85% yield with complete selectivity (Fig. 4e).

Synthetic applications

To showcase the synthetic utility of this discovery, gram-scale reactions of quinolone **1j** were first performed under both reaction conditions, and products **3ja** and **4ja** were isolated in 96% and 85% yields without erosion of the regioselectivity (Fig. 5a). Further derivatizations of **3ja** were achieved with synthetically useful intermediate **8**, which was obtained in 70% yield by the TBAF-mediated removal of the TIPS group. For instance, hydrogenation of **8** under 1 atm of hydrogen with a catalytic amount of Pd/$BaCO_3$ yielded alkylation product **9a** in high yield. The use of the Wilkinson catalyst for hydrogenation allowed for the chemoselective synthesis of olefin **9b**. The terminal triple bond in **8** could be effectively transformed into an internal bond to provide product **9c** in nearly quantitative conversion through the Sonogashira reaction. Ag catalysis of the reaction of **8** with NBS formed bromination product **9d** in excellent yield. In addition, alkyne **8** was easily converted to triazole **9e** with BnN_3 via a copper-catalysed click reaction. Based on diverse alkyne conversion, our strategy provides a simple and distinct way to construct a number of pharmaceutically relevant compounds and materials. The reaction of quinoline **10** under Conditions B furnished C2-alkynylation, and further removal of the

https://doi.org/10.1038/s41467-023-39753-2

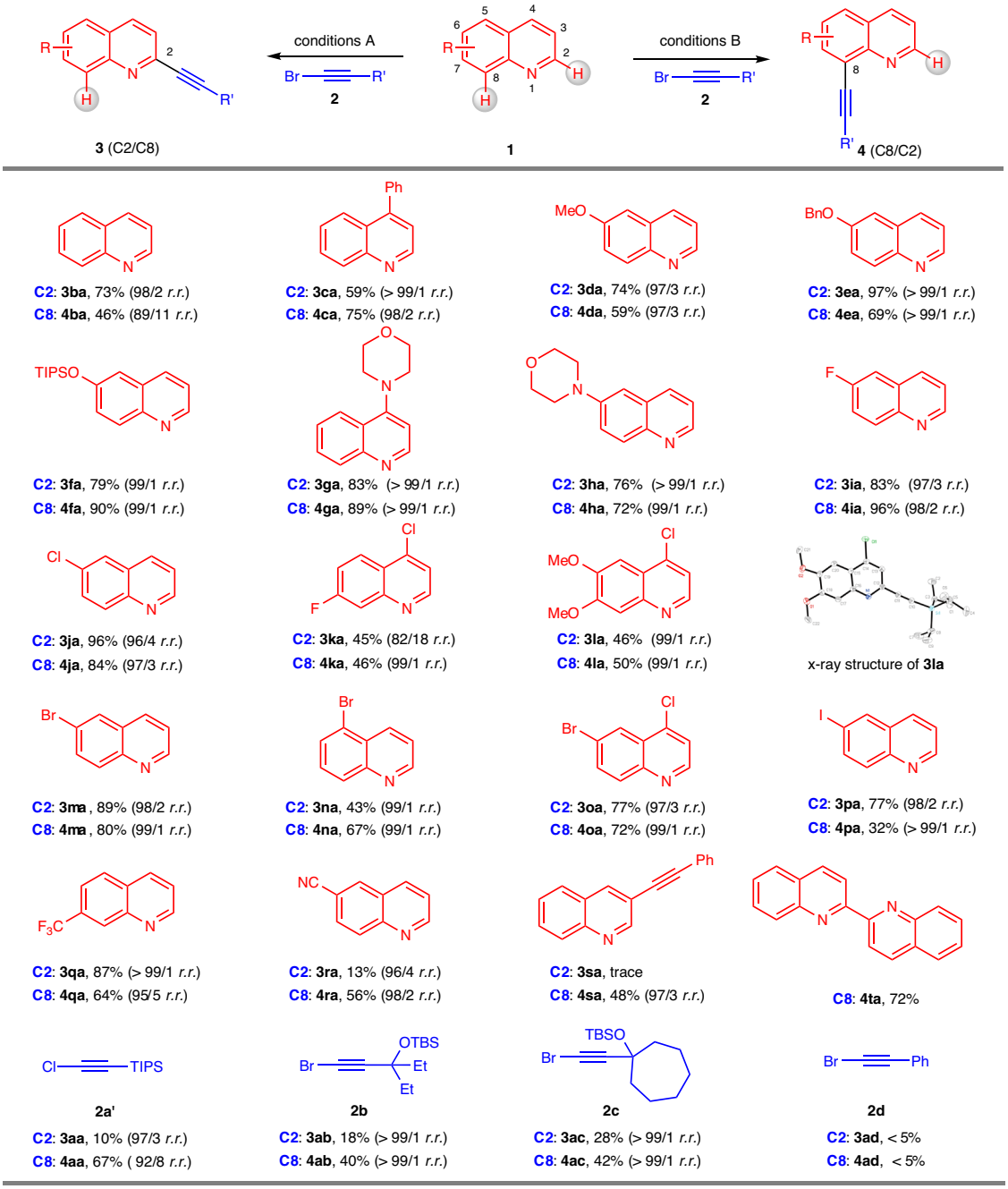

Fig. 3 | Substrate scope of the regiodivergent C–H alkynylation of quinolines at the C2 and C8 positions. Reaction Conditions A: $[Rh(cod)Cl]_2$ (5 mol%), dtbpy (10 mol%), **1** (0.20 mmol, 1.0 equiv), **2** (0.50 mmol, 2.5 equiv), NaO^{t}Bu (0.50 mmol, 2.5 equiv), 1 mL of toluene, 120 °C, 12 h, under argon. Reaction Conditions B: [Rh(cod)(IMes)Cl (10 mol%), **1** (0.20 mmol, 1.0 equiv), **2** (0.50 mmol, 2.5 equiv), NaO^{t}Bu (0.50 mmol, 2.5 equiv), 1 mL of toluene, 120 °C, 12 h, under argon. r.r. values were determined by GC–MS analysis of the reaction mixture.

TIPS group provided Compound **11** in good yield, acting as a core framework for the tautomerase inhibitor (Fig. 5b). As a key intermediate for the synthesis of montelukast, Compound **13** was rapidly prepared from quinoline **12** by C2-selective C–H alkynylation with bromoalkyne **2a**, further removal of the TIPS group and reduction with the Wilkinson catalyst under 1 atm of hydrogen (Fig. 5c). Compound **15** is a key intermediate in the synthesis of BN-dibenzo[a,o]picene, and 3,8-dibromo-4,7-phenanthroline (**14**) must be pregenerated through multistep synthesis from **5c** to access this molecule by Sonogashira coupling (Fig. 5d)[60]. Notably, this molecule can be prepared in an atom- and step-economic way, further indicating the value of the developed method.

Mechanistic study

In order to gain insights into the reaction pathways and origin of positional selectivity, density functional theory (DFT) calculations were performed using the reaction of quinoline **1b** and alkynyl bromide **2a** as the model (Fig. 6). The reaction initially commences by the formation of **1b** and the ligand bound Rh(I) intermediate **INT1A**, which is set as the relative zero point of the Gibbs free energy. The previous reported Rh(I)-involved C–H activation by oxidative addition might be a reversible process with an activation energy barrier of 26.2 kcal mol^{-1} (for the details of the computational data, see the Supplementary Information)[36–38]. Comparably, **INT1A** more favorably coordinates with **2a** to generate **INT2A**, which then undergoes C–Br bond oxidative

https://doi.org/10.1038/s41467-023-39753-2

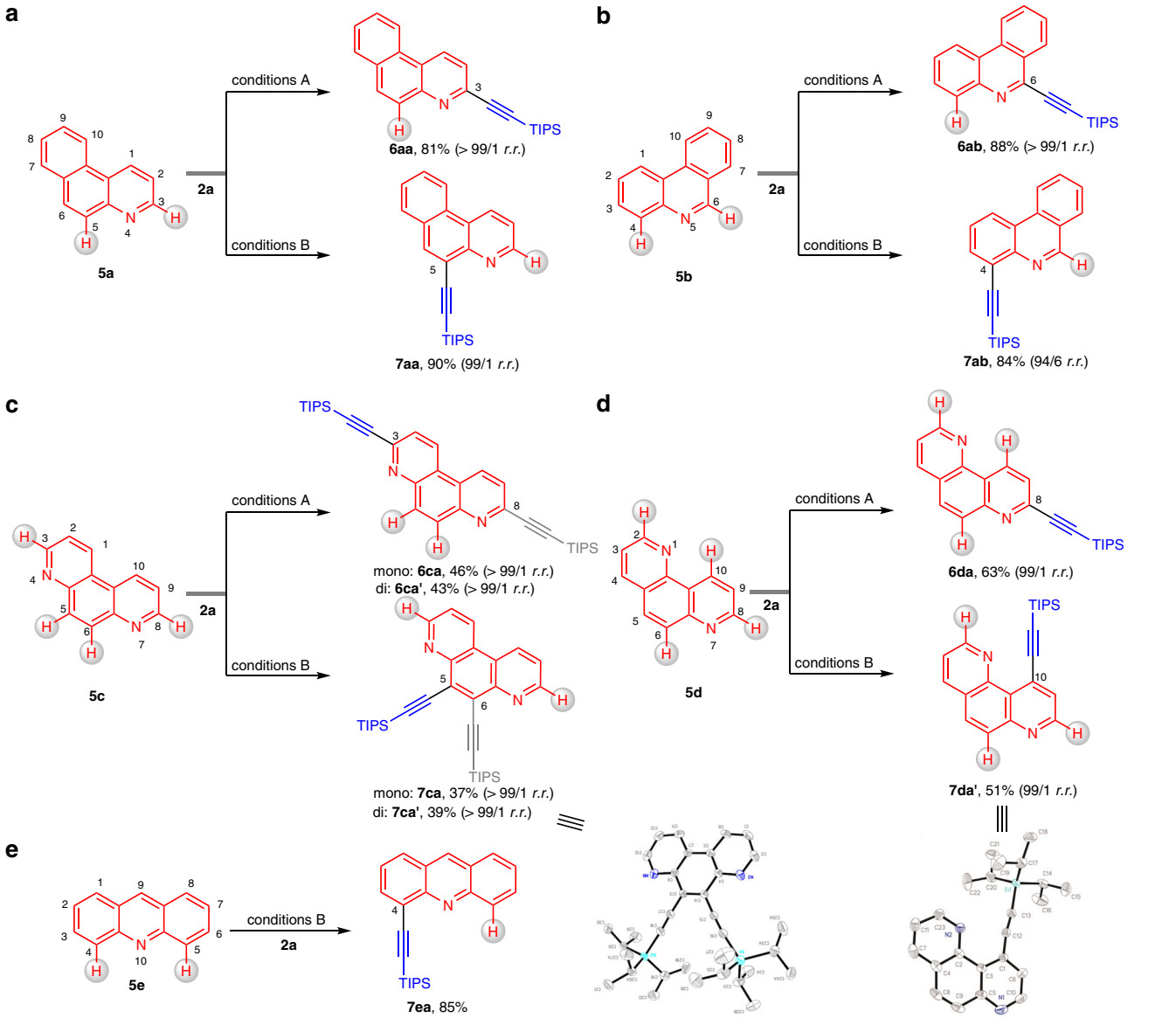

Fig. 4 | Regiodivergent C–H alkynylation of diverse aza-arenes. a C–H alkynylation of benzo[*f*]quinolone (**5a**). **b** C–H alkynylation of phenanthridine (**5b**). **c** C–H Alkynylation of 4,7-phenanthroline (**5c**). **d** C–H alkynylation of 1,7-phenanthroline (**5d**). **e** C–H alkynylation of acridine (**5e**).

addition to afford Rh(III) species **INT3A**. In the case of the dtbpy ligand, the C–Br oxidative addition through transition state **TS3A-dtbpy** was calculated to have an activation free energy of 27.6 kcal mol^{-1}. This step is the rate-determining step in the catalytic cycle. The resulting intermediate **INT3A-dtbpy** occurs C2–H metalation through a ^{t}butoxide-assisted deprotonation with a 25.8 kcal mol^{-1} energy barrier[61–66]. Further reductive elimination and ligand exchange yield the desired products with high selectivity and regenerates **INT1A** to complete the catalytic cycle. For the IMes ligand, the C–Br bond oxidative addition to the Rh(I) center from **INT2A-IMes** has an activation energy of 26.7 kcal mol^{-1}, which shows a comparable energy barrier with the subsequent C–H activation (26.1 kcal mol^{-1}). In the following C – H metalation, IMes ligand favors C8 selective transition state **TS4B-IMes**.

As shown in Fig. 7, extensive computational studies on different site selectivity were also carried out. The molecular electrostatic potential map was used to analysis the possible nucleophilic sites of quinoline **1b** (Fig. 7a). Quantitatively, the natural population analysis of **1a** shows that C2 has an atomic charge of −0.069e, which is less charged than C8 (−0.192e), illustrating C2 – H is relative electron deficient and more prone to C – H metallization with electron-rich rhodium catalyst (Supplementary Data 1). Inspecting computed electrostatic potential maps of **Rh–dtbpy** and **Rh–IMes**, the dtbpy ligand exhibits more electron-donating ability than IMes, allowing **INT3A-dtbpy** to preferentially react with the C2 position of **1b**. The energy barrier of the rhodacycle transition state **TS4A-dtbpy** that delivers the three-membered intermediate **INT4A-dtbpy** is 8.2 kcal mol^{-1} lower than that of the competing transition state **TS4B-dtbpy** that leads to the **INT4B-dtbpy** (Fig. 7b). This energy difference is consistent with the experimentally excellent site selectivity of **3ba**. Without the nitrogen chelation, transition states **TS4C-dtbpy** and **TS4D-dtbpy** have activation barriers of 42.0 and 43.9 kcal mol^{-1}, respectively. Such high computed energies are mainly ascribed to the intrinsic inertness of the C – H bonds at the C2 and C8 position of quinoline, indirectly illustrating the importance of the directing group. The directed C–H metalation transition state

https://doi.org/10.1038/s41467-023-39753-2

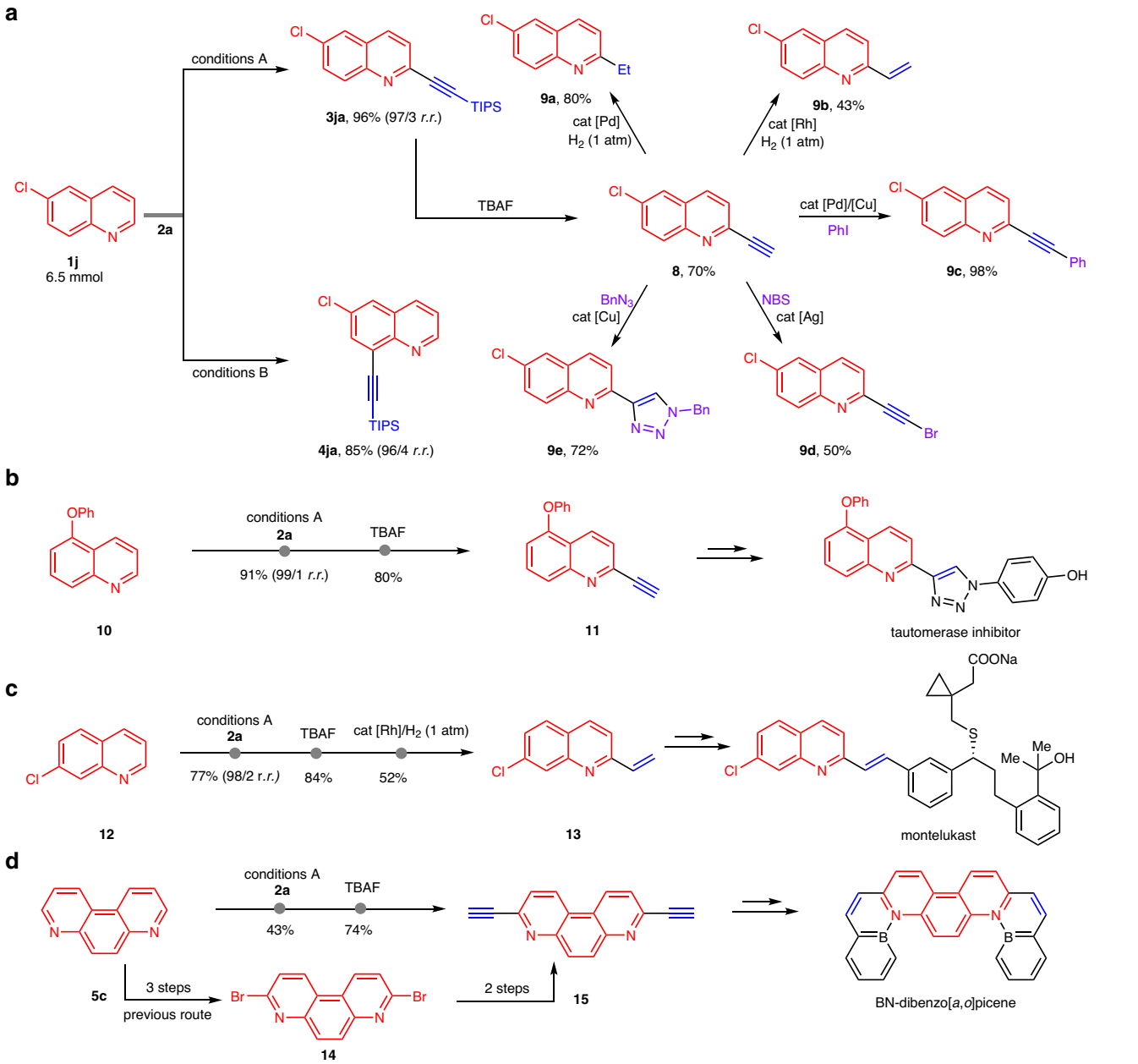

Fig. 5 | Synthetic applications of regiodivergent C–H alkynylation. a Gram-scale preparation of **3ja** and **4ja** and their derivatizations. **b** Application of the process to the synthesis of potent tautomerase inhibitors. **c** Application of the process to the synthesis of montelukast. **d** Application of the process to the synthesis of BN-dibenzo[a,o]picene.

through **TS4B-IMes** has an activation Gibbs free energy of 26.1 kcal mol^{-1}, which is 17.3 kcal mol^{-1} lower than the same process through **TS4A-IMes** (26.1 and 43.4 kcal mol^{-1}) and 11.2 kcal mol^{-1} lower than the original nucleophilic attack at quinoline C2 position through **TS4C-IMes** (26.1 and 37.3 kcal mol^{-1}). In addition, the steric maps around the Rh(III) centre with IMes ligand were analyzed based on the SambVca 2.1 tool (Fig. 7c)[65,66]. All transition states adopt trigonal bipyramidal geometries, where Br atom and O^{t}Bu group occupy the two vertex positions and the IMes ligand in the NW quadrant of the steric map extends to the NE and SW quadrants. In disfavored transition state **TS4A-IMes**, bicyclo 3-4 fused rhodacycle enables the Rh–C bond formation to occur in the SW quadrant, which suffers from significant repulsion with Mes group of the carbene ligand. The favored transition state **TS4B-IMes** is a bicyclo 4-4 fused rhodacycle, the expansion of ring size makes the quinoline backbone more horizontally extended and reduce the steric hindrance between quinoline and TIPS group, thereby effectively lowering the energy barrier of **TS4B-IMes**. In **TS4C-IMes** and **TS4D-IMes**, Rh–N bond distances are elongated to 2.85 and 3.57 Å, respectively, indicating nitrogen atom in **1b** is not anchored around the Rh(III) centre. Taken together, the electronic and steric effects account for the tunability of the strained metallacycles, achieving different positional selectivity[67,68].

Discussion

In conclusion, the present results demonstrate an important initial advance in C–H activation through a benzo-fused three- or four-membered ring cyclometallation pathway in a switchable mode. This

https://doi.org/10.1038/s41467-023-39753-2

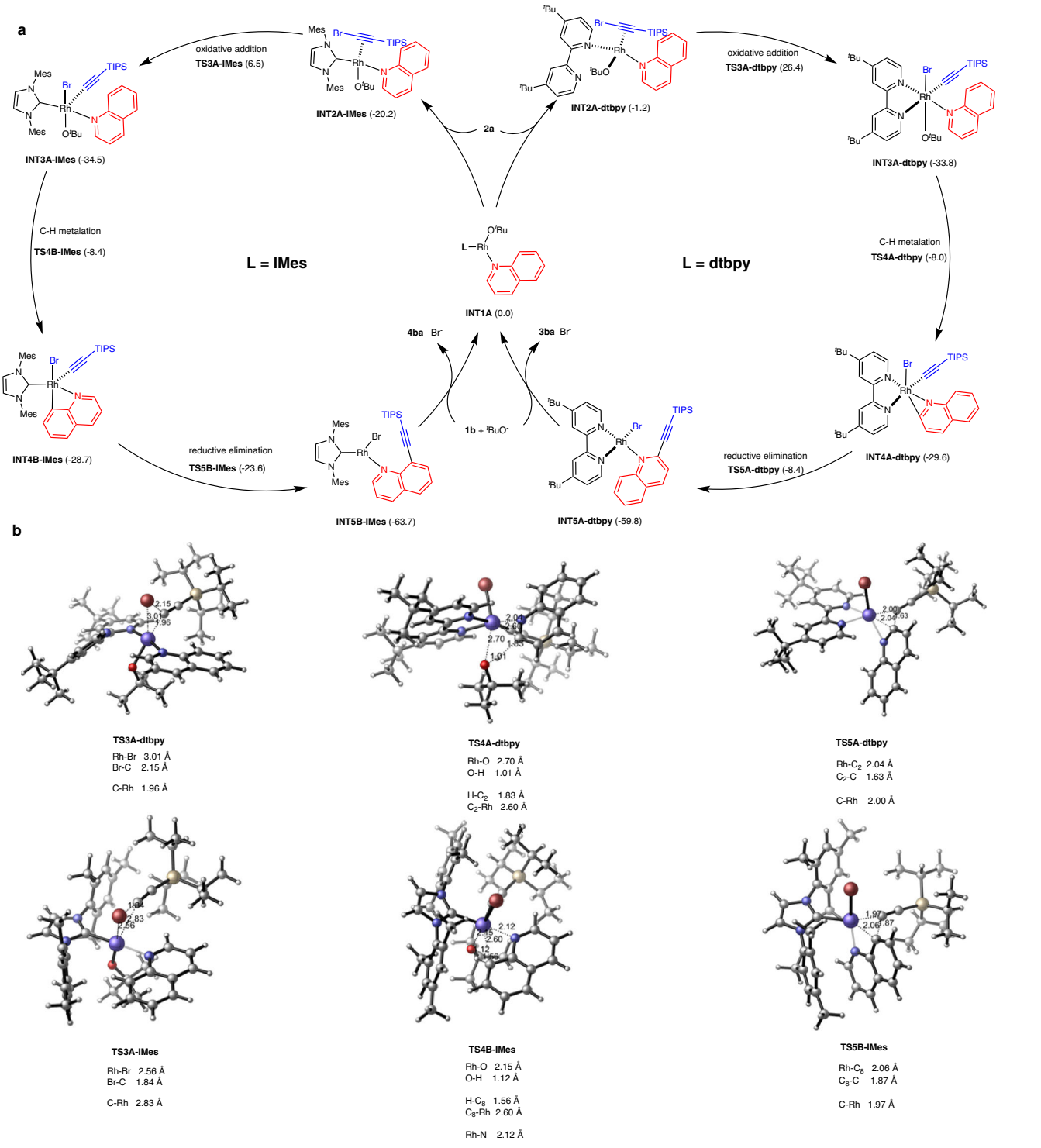

Fig. 6 | Calculated energy profiles of the regiodivergent C–H alkynylation of 1b with 2a. a The proposed catalytic cycles with different ligands. **b** The key transition states in the catalytic cycle.

chemistry provides a unique tool for the functionalization of high-value aza-arenes with divergent site selectivities controlled by ligands. The switch of the positional selectivity through strained metallacycles fills a major methodological gap in directed C–H activation. We anticipate that other transformations based on this strategy could be exploited for molecular editing of aza-arene C–H bonds, providing inspiration for the design of new tactics to produce complex bioactive molecules, natural products and functional materials.

Methods

Due to slight variations in experimental protocols for all the processes we present, we refer the reader to the Supplementary Methods for experimental details.

Data availability

Crystallographic data for the structures of Rh(cod)(dtbpy)Cl, Rh(cod)(IMes)Cl, **3ia**, **7ca'** and **7da'** reported in this paper have been deposited at the Cambridge Crystallographic Data Centre under

https://doi.org/10.1038/s41467-023-39753-2

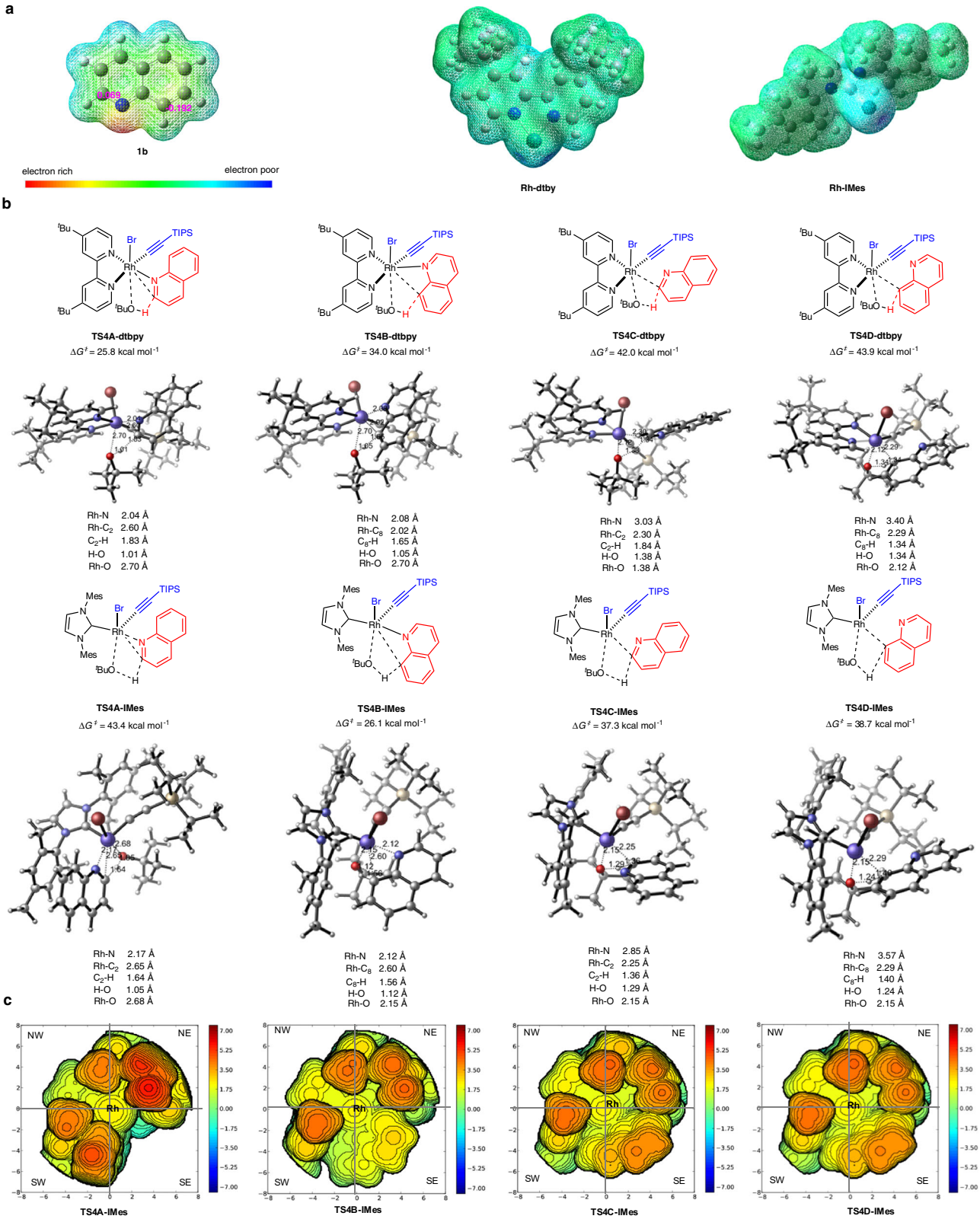

Fig. 7 | The origin of the site selectivity. a Molecular electrostatic potential map of **1b**, **Rh–dtbpy**, and **Rh–IMes**. **b** Key transition states for the different site selectivities. **c** Steric maps of the Rh(III) transition states **TS4A-IMes**, **TS4B-IMes**, **TS4C-IMes**, and **TS4D-IMes**.

deposition numbers CCDC 2192163, 2192164, 2192165, 2192166 and 2192167 (Supplementary Data 2). Copies of the data can be obtained free of charge via www.ccdc.cam.ac.uk/getstructures. All other data supporting the findings of the study, including experimental procedures and compound characterization, are available within the paper and its Supplementary Information, or from the corresponding author upon reasonable request.

References

1. Bergman, R. G. C–H activation. *Nature* **446**, 391–393 (2007).
2. Wencel-Delord, J., Dröge, T., Liu, F. & Glorius, F. Towards mild metal-catalyzed C–H bond activation. *Chem. Soc. Rev.* **40**, 4740–4761 (2011).
3. Dong, Z. et al. Transition-metal-catalyzed C–H alkylation using alkenes. *Chem. Rev.* **117**, 9333–9403 (2017).
4. Yang, Y., Lan, J. & You, J. Oxidative C–H/C–H coupling reactions between two (hetero)arenes. *Chem. Rev.* **117**, 8787–8863 (2017).
5. Wang, C.-S., Dixneuf, P. H. & Soulé, J.-F. Photoredox catalysis for building C–C bonds from C(sp^2)–H bonds. *Chem. Rev.* **118**, 7532–7585 (2018).
6. Davies, H. M. L. & Liao, K. Dirhodium tetracarboxylates as catalysts for selective intermolecular C–H functionalization. *Nat. Rev. Chem.* **3**, 347–360 (2019).
7. Gandeepan, P. et al. 3d Transition metals for C–H activation. *Chem. Rev.* **119**, 2192–2452 (2019).
8. Guillemard, L., Kaplaneris, N., Ackermann, L. & Johansson, M. J. Late-stage C–H functionalization offers new opportunities in drug discovery. *Nat. Rev. Chem.* **5**, 522–545 (2021).
9. Zhao, B., Prabagar, B. & Shi, Z. Modern strategies for C–H functionalization of heteroarenes with alternative coupling partners. *Chemistry* **7**, 2585–2634 (2021).
10. Dalton, T., Faber, T. & Glorius, F. C–H Activation: Toward sustainability and applications. *ACS Cent. Sci.* **7**, 245–261 (2021).
11. Giri, R. et al. Transition metal-catalyzed C–H activation reactions: diastereoselectivity and enantioselectivity. *Chem. Soc. Rev.* **38**, 3242–3272 (2009).
12. Wright, J. S., Scott, P. J. H. & Steel, P. G. Iridium-catalysed C–H borylation of heteroarenes: balancing steric and electronic regiocontrol. *Angew. Chem. Int. Ed.* **60**, 2796–2821 (2021).
13. Lyons, T. W. & Sanford, M. S. Palladium-catalyzed ligand-directed C–H functionalization reactions. *Chem. Rev.* **110**, 1147–1169 (2010).
14. Colby, A. A., Bergman, R. G. & Ellman, J. A. Rhodium-catalyzed C–C bond formation via heteroatom-directed C–H bond activation. *Chem. Rev.* **110**, 624–655 (2010).
15. Zhang, F. & Spring, D. R. Arene C–H functionalisation using a removable/modifiable or a traceless directing group strategy. *Chem. Soc. Rev.* **43**, 6906–6919 (2014).
16. Sambiagio, C. et al. A comprehensive overview of directing groups applied in metal-catalysed C–H functionalisation chemistry. *Chem. Soc. Rev.* **47**, 6603–6743 (2018).
17. Liu, B. et al. Transition-metal-catalyzed, coordination-assisted functionalization of nonactivated C(sp^3)–H bonds. *Chem. Rev.* **121**, 14957–15074 (2021).
18. Leow, D., Li, G., Mei, T.-S. & Yu, J.-Q. Activation of remote *meta*-C–H bond assisted by an end-on template. *Nature* **486**, 518–522 (2012).
19. Tang, R., Li, G. & Yu, J.-Q. Conformation-induced remote *meta*-C–H activation of amines. *Nature* **507**, 215–220 (2014).
20. Xu, H.-J. et al. Rh(III)-catalyzed *meta*-C–H alkenylation with alkynes. *J. Am. Chem. Soc.* **141**, 76–79 (2019).
21. Dutta, U., Maiti, S., Bhattacharya, T. & Maiti, D. Arene diversification through distal C(sp^2)–H functionalization. *Science* **372**, eabd5992 (2021).
22. Dutta, U. & Maiti, D. Emergence of pyrimidine-based meta-directing group: Journey from weak to strong coordination in diversifying *meta*-C–H functionalization. *Acc. Chem. Res.* **55**, 354–372 (2022).
23. He, C., Whitehurst, W. G. & Gaunt, M. J. Palladium-catalyzed C(sp^3)–H bond functionalization of aliphatic amines. *Chem* **5**, 1031–1058 (2019).
24. Trowbridge, A., Walton, S. M. & Gaunt, M. J. New strategies for the transition-metal catalyzed synthesis of aliphatic amines. *Chem. Rev.* **120**, 2613–2692 (2020).
25. Herzon, S. B. & Hartwig, J. F. Direct, Catalytic hydroaminoalkylation of unactivated olefins with N-alkyl arylamines. *J. Am. Chem. Soc.* **129**, 6690–6691 (2007).
26. Koperniku, A., Foth, P. J., Sammis, G. M. & Schafer, L. L. Zirconium hydroaminoalkylation. An alternative disconnection for the catalytic synthesis of α-arylated primary amines. *J. Am. Chem. Soc.* **141**, 18944–18948 (2019).
27. Manßen, M. & Schafer, L. L. Titanium catalysis for the synthesis of fine chemicals—development and trends. *Chem. Soc. Rev.* **49**, 6947–6994 (2020).
28. DiPucchio, R. C. et al. Direct, catalytic α-alkylation of N-heterocycles by hydroaminoalkylation: Substrate effects for regiodivergent product formation. *J. Am. Chem. Soc.* **143**, 11243–11250 (2021).
29. Manßen, M. & Schafer, L. L. Early transition metal-catalyzed hydroaminoalkylation. *Trends Chem.* **3**, 428–429 (2021).
30. DiPucchio, R. C., Rosca, S.-C. & Schafer, L. L. Hydroaminoalkylation for the catalytic addition of amines to alkenes or alkynes: Diverse mechanisms enable diverse substrate scope. *J. Am. Chem. Soc.* **144**, 11459–11481 (2022).
31. McNally, A., Haffemayer, B., Collins, B. S. L. & Gaunt, M. J. Palladium-catalysed C–H activation of aliphatic amines to give strained nitrogen heterocycles. *Nature* **510**, 129–133 (2014).
32. He, C. & Gaunt, M. J. Ligand-enabled catalytic C–H arylation of aliphatic amines by a four-membered ring cyclopalladation pathway. *Angew. Chem. Int. Ed.* **54**, 15840–15844 (2015).
33. Willcox, D. et al. A general catalytic β-C–H carbonylation of aliphatic amines to β-lactams. *Science* **354**, 851–857 (2016).
34. Stephens, D. E. & Lariono, O. V. Recent advances in the C–H-functionalization of the distal positions in pyridines and quinolones. *Tetrahedron* **71**, 8683–8716 (2015).
35. Prabagar, B., Yang, Y. & Shi, Z. Site-Selective C–H functionalization to access the arene backbone of indoles and quinolines. *Chem. Soc. Rev.* **50**, 11249–11269 (2021).
36. Lewis, J. C., Bergman, R. G. & Ellman, J. A. Rh(I)-Catalyzed alkylation of quinolines and pyridines *via* C–H bond activation. *J. Am. Chem. Soc.* **129**, 5332–5333 (2007).
37. Berman, A. M., Lewis, J. C., Bergman, R. G. & Ellman, J. A. Rh(I)-catalyzed direct arylation of pyridines and quinolines. *J. Am. Chem. Soc.* **130**, 14926–14927 (2008).
38. Berman, A. M., Bergman, R. G. & Ellman, J. A. Rh(I)-catalyzed direct arylation of azines. *J. Org. Chem.* **75**, 7863–7868 (2010).
39. Ye, M., Gao, G.-L. & Yu, J.-Q. Ligand-promoted C-3 selective C–H olefination of pyridines with Pd catalysts. *J. Am. Chem. Soc.* **133**, 6964–6967 (2011).
40. Nakao, Y., Yamada, Y., Kashihara, N. & Hiyama, T. Selective C-4 alkylation of pyridine by nickel/Lewis acid catalysis. *J. Am. Chem. Soc.* **132**, 13666–13668 (2010).
41. Tsai, C.-C. et al. Bimetallic nickel aluminun mediated para-selective alkenylation of pyridine: direct observation of η2,η1-pyridine Ni(0)-Al(iii) intermediates prior to C–H bond activation. *J. Am. Chem. Soc.* **132**, 11887–11889 (2010).
42. Kim, J. H. et al. A radical approach for the selective C–H borylation of azines. *Nature* **595**, 677–683 (2021).
43. Zhang, X. et al. Phosphorus-mediated sp^2–sp^3 couplings for C–H fluoroalkylation of azines. *Nature* **594**, 217–222 (2021).
44. Hwang, H., Kim, J., Jeong, J. & Chang, S. Regioselective introduction of heteroatoms at the C-8 position of quinoline N-oxides: Remote C–H activation using N-oxide as a stepping stone. *J. Am. Chem. Soc.* **136**, 10770–10776 (2014).

45. Shukla, R. K., Nair, A. M., Khan, S. & Volla, C. M. R. Cobalt-catalyzed C8-dienylationof quinoline-N-oxides. *Angew. Chem. Int. Ed.* **59**, 17042–17048 (2020).
46. Stephens, D. E. et al. Palladium-catalyzed C8-selective C–H arylation of quinoline N-oxides: insights into the electronic, steric, and solvation effects on the site selectivity by mechanistic and DFT computational studies. *ACS Catal.* **5**, 167–175 (2015).
47. Shapley, J. R., Samkoff, D. E., Bueno, C. & Churchill, M. R. Reaction of Os3(CO)10(NCCH3)2 with imidazole and related aromatic heterocycles. The crystal and molecular structure of (.mu.-H)Os3(CO)10 (.mu.-3,4-.eta.2-N2C3H3. *Inorg. Chem*. 21, 634–639 (1982).
48. Fukuyama, T. et al. $Ru_3(CO)_{12}$-Catalyzed site-selective carbonylation reactions at a C–H Bond in aza-heterocycles. *J. Am. Chem. Soc.* **120**, 11522–11523 (1998).
49. Kwak, J., Kim, M. & Chang, S. Rh(NHC)-catalyzed direct and selective arylation of quinolines at the 8-position. *J. Am. Chem. Soc.* **133**, 3780–3783 (2011).
50. Zhang, Z., Tanaka, K. & Yu, J.-Q. Remote site-selective C–H activation directed by a catalytic bifunctional template. *Nature* **543**, 538–542 (2017).
51. Ramakrishna, K. et al. Coordination assisted distal C–H alkylation of fused heterocycles. *Angew. Chem. Int. Ed.* **58**, 13808–13812 (2019).
52. Shi, H. et al. Differentiation and functionalization of remote C–H bonds in adjacent positions. *Nat. Chem.* **12**, 399–404 (2020).
53. Fan, Z. et al. Molecular editing of aza-arene C–H bonds by distance, geometry and chirality. *Nature* **610**, 87–93 (2022).
54. Zhao, Q., Meng, G., Nolan, S. P. & Szostak, M. N-Heterocyclic carbene complexes in C–H activation reactions. *Chem. Rev.* **120**, 1981–2048 (2020).
55. Ano, Y., Tobisu, M. & Chatani, N. Palladium-catalyzed direct ethynylation of $C(sp^3)$–H bonds in aliphatic carboxylic acid derivatives. *J. Am. Chem. Soc.* **133**, 12984–12986 (2011).
56. He, J., Wasa, M., Chan, K. S. L. & Yu, J.-Q. Palladium(0)-catalyzed alkynylation of $C(sp^3)$–H bonds. *J. Am. Chem. Soc.* **135**, 3387–3390 (2013).
57. Viart, H. M.-F., Bachmann, A., Kayitare, W. & Sarpong, R. β-Carboline amides as intrinsic directing groups for $C(sp^2)$–H functionalization. *J. Am. Chem. Soc.* **139**, 1325–1329 (2017).
58. Liao, G. et al. Scalable, Stereocontrolled formal syntheses of (+)-Isoschizandrin and (+)-Steganone: Development and applications of palladium(II)-catalyzed atroposelective C–H alkynylation. *Angew. Chem. Int. Ed.* **57**, 3661–3665 (2018).
59. Mondal, A. et al. Sterically controlled late-stage C–H alkynylation of arenes. *J. Am. Chem. Soc.* **141**, 18662–18667 (2019).
60. Neue, B., Araneda, J. F., Piers, W. E. & Parvez, M. BN-Dibenzo[a,o]picenes: analogues of an unknown polycyclic aromatic hydrocarbon. *Angew. Chem. Int. Ed.* **52**, 9966–9969 (2013).
61. Qi, X., Li, Y., Bai, R. & Lan, Y. Mechanism of rhodium-catalyzed C–H functionalization: advances in theoretical investigation. *Acc. Chem. Res.* **50**, 2799–2808 (2017).
62. Davies, D. L., Macgregor, S. A. & McMullin, C. L. Computational studies of carboxylate-assisted C–H activation and functionalization at group 8–10 transition metal centers. *Chem. Rev.* **117**, 8649–8709 (2017).
63. Lapointe, D. & Fagnou, K. Overview of the mechanistic work on the concerted metallation-deprotonation pathway. *Chem. Lett.* **39**, 1118–1126 (2010).
64. Funes-Ardoiz, I. & Maseras, F. Oxidative coupling mechanisms: current state of understanding. *ACS Catal.* **8**, 1161–1172 (2018).
65. Balcells, D., Clot, E. & Eisenstein, O. C–H bond activation in transition metal species from a computational perspective. *Chem. Rev.* **110**, 749–823 (2010).
66. Jiang, Y.-Y., Man, X. & Bi, S. Advances in theoretical study on transition-metal-catalyzed C–H activation. *Sci. China: Chem.* **59**, 1448–1466 (2016).
67. Falivene, L. et al. Towards the online computer-aided design of catalytic pockets. *Nat. Chem.* **11**, 872–879 (2019).
68. Falivene, L. et al. SambVca 2. A web tool for analyzing catalytic pockets with topographic steric maps. *Organometallics* **35**, 2286–2293 (2016).

Acknowledgements

We would like to thank the National Natural Science Foundation of China (Grants 22025104, 22171134, 21972064, and 21901111), the Fundamental Research Funds for the Central Universities (Grant 020514380254) for their financial support and Tang Scholar. We are also grateful to the High-Performance Computing Center of Nanjing University for performing the numerical calculations in this paper on its blade cluster system.

Author contributions

L.X. developed the catalysts and reactions and performed and analyzed experiments. M.W. performed the DFT calculation. Y.L. supervised the DFT calculation and commented on the manuscript. Y.Z. performed the crystallographic studies; Z.S. conceived and supervised the project and wrote the manuscript.

Competing interests

The authors declare no competing interests.

Additional information

Supplementary information The online version contains supplementary material available at https://doi.org/10.1038/s41467-023-39753-2.

Correspondence and requests for materials should be addressed to Zhuangzhi Shi.

Peer review information *Nature Communications* thanks the anonymous reviewers for their contribution to the peer review of this work.